J Mater Sci: Mater Electron (2022) 33:22728–22735

Effects of flash annealing and external magnetic field on magnetic properties of relatively high Nd content (37% by weight) NdFeB alloy

Muhammed Fatih Kılıçaslan[1,*], Yasin Yılmaz[2], Bekir Akgül[2], and Hasan Tiryaki[3]

[1] Department of Fundamental Sciences and Engineering, Sivas University of Science and Technology, Sivas, Turkey
[2] Department of Aeronautical Engineering, Sivas University of Science and Technology, Sivas, Turkey
[3] Department of Electrical and Electronic Engineering, Istanbul University, Cerrahpaşa, Istanbul, Turkey

Received: 19 May 2022
Accepted: 23 August 2022
Published online: 26 September 2022

ABSTRACT

Post modifications such as alloying element addition and/or heat treatment are applied to improve the magnetic properties of NdFeB permanent magnets. In this study, effects of external magnetic field and flash annealing at different temperatures (680 °C and 710 °C) and durations of 5 and 10 min on the magnetic properties of relatively high Nd content (37 wt.%) NdFeB magnet alloys were investigated. Melt spinning method was used in production of the NdFeB magnet alloys. Heat treatment was applied to various NdFeB magnet ribbons at 680 °C and 710 °C temperatures for 5 and 10 min by the flash annealing at heating and cooling rates of 300 K/s. In addition, before vibrating sample magnetometer tests, various samples were magnetized under an external magnetic field of 5 Tesla. After melt spinning, semi-amorphous structure was obtained and Nd2Fe14B hard and α-Fe soft magnetic phases were crystallized at nanoscale by flash annealing. These crystallizations formed between approximately 350 °C and 430 °C. After the flash annealing, residual amorphous structures were observed without complete crystallization. The highest remanence and coercivity were obtained in the sample flash annealed for 10 min at 710 °C, 57.64 emu/g and 10,419.07 Oe, respectively. The maximum energy product improved thanks to the high remanence and coercivity, important for the NdFeB magnets resulted in a high value of 87.79 kJ/m^3 in the same sample. This flash annealing procedure provides a cost-effective and simple platform to improve the magnetic features of NdFeB magnets.

Address correspondence to E-mail: fatihkilicaslan@sivas.edu.tr

https://doi.org/10.1007/s10854-022-08992-2

1 Introduction

Permanent magnets are the fundamental components of many electrical, electronic and electro-mechanical devices. It's widely used in today's technologically developed societies [1, 2]. In this materials, it is aimed to provide large magnetic fields without consuming electrical energy or releasing thermal energy [1–3]. The permanent magnet materials can be examined in four different groups as AlNiCo alloys, ferrites, rare earth cobalt alloys (Sm–Co) and rare earth-iron alloys (NdFeB) [1, 4]. Among these, NdFeB compound was found in the 1980s and various methods have been used to improve their physical properties such as magnetic and thermal [1, 5–9]. NdFeB magnets have high spontaneous polarization ($J_s > 1.2$ T) and crystalline anisotropy (Kl > 106 J/m^3), all of which provide a high maximum energy product ($BH_{max} > 450$ kJ/m^3) [7, 10–12]. These superior magnetic properties make them widely used in several commercial applications [3, 6, 13–18]. NdFeB permanent magnets have been widely applied in various fields, such as electronic and aerospace industry, information and medical equipment, hybrid electric vehicles (HEVs) and wind generators by changing coercivity and maximum energy product [6, 19]. In this context, NdFeB-based permanent magnets play an important role in reducing the size of products (motor etc.) in applications where high efficiency is required. The global permanent magnets market share was valued at $17.33 billion in 2018 and is expected to reach $30.67 billion by 2025 [20].

Considering the increasing global needs, the demand for NdFeB magnets with high energy product and coercivity is increasing day by day. For this, the first stage is the production method. Some of the methods used in the production of NdFeB-based permanent magnetic materials with hard magnetic properties are powder metallurgical methods (sintered magnets), rapid cooling methods such as melt spinning, severe plastic deformation, mechanical alloying, HDDR [7, 11, 18, 21–23]. Among these, the melt spinning, which is one of the rapid solidification methods, it is possible to obtain an amorphous and relatively fine-grained microstructure [22] and, as a result, superior magnetic properties at high cooling rates [5]. As known, in the melt spinning method, atoms crystallize in nano-size crystal order or amorphous depending on the cooling rate, due to the effect of rapid solidification [24, 25]. The formation of an amorphous, semi-amorphous or crystalline structure depends on the parameters, affecting the cooling rate in the melt spinning method [26, 27]. Grains refined with melt spinning make a significant contribution to the magnetic properties of NdFeB magnet alloys [24]. As it is known, grain size should be below 3 μm for high coercivity [28, 29]. These grain sizes can be reached as follows; (i) nano-sized grains can be formed by optimizing melt spinning parameters [26] or (ii) obtained by flash annealing of amorphous or semi-amorphous ribbons after melt spinning [5, 25, 30, 31]. The temperature and durations required for the flash annealing process can be determined by considering atomic diffusion [5, 25, 30]. As a result, by refining the grain size, the coercivity and magnetic remanence, and accordingly the energy product increases.

Moreover, the NdFeB magnets contain about 32–35 wt% rare earth elements (REEs), mainly Nd. Depending on their application areas, as well as heavy rare earth elements (HREEs) such as Dy, Tb and Ga, which are small but expensive [19]. In addition, sources of HREEs such as Dy, Tb and Ga are both very few in the world and their reserves are decreasing day by day [6, 32, 33]. With the expansion of application areas of NdFeB-based magnets, the need for continuous improvement of their magnetic performance is increasing [7]. Therefore, many researchers have tried to increase the magnetic properties of NdFeB magnets without using HREEs [34, 35]. For this purpose, first of all, it was tried to increase the coercivity and energy product by changing the amount of Nd [24, 29, 35]. It is known that the coercivity and energy product improve with the increase of Nd amount [29, 35]. Because the Nd promotes further formation of $Nd_2Fe_{14}B$ hard magnetic phase in the structure [29]. Therefore, in our study, we chose the amount of Nd 37% by weight, without using HRREs such as Dy, Tb and Ga. To our best knowledge, it is the first time in the literature to study NdFeB-based magnets with relatively high Nd content. In addition, the melt spinning method was used to obtain amorphous and/or semi-amorphous structures. In order to reach nano-sized grains, flash annealing were applied to the amorphous ribbons under different conditions (different temperature and durations). As it is known, heat treatments improve magnetic properties of NdFeB magnets [28, 31, 36]. Therefore, to avoid compromising the nanoparticle size, the samples were rapidly heated to 680 °C and

710 °C and held for 5–10 min and then rapidly cooled. In addition, an external magnetic field of 5 Tesla was applied to various samples. As a result of our studies, the highest coercivity value was obtained as 10,667.98 Oe in the sample without heat treatment and magnetic field. The maximum energy product was 87.79 kJ/m^3, in the sample which flash annealed at 710 °C for 10 min.

2 Experimental

NdFeB-based ingot alloys were produced in a vacuum induction melting (VIM) furnace under high vacuum (10–4 mbar) and argon atmosphere (500 mbar partial argon pressure), and their nominal chemical compositions are listed in Table 1. Chemical composition of NdFeB-based magnet alloys was determined using a Bruker S2 PUMA X-ray fluorescence spectrometer (XRF). For each ingot alloy produced, the VIM process was repeated three times to ensure homogeneity. The ingots are produced to have a weight of 200 g. Approximately 20 g samples were used from the ingots produced for melt spinning. The liquid metal, which was remelted under vacuum, was sprayed from a 1 × 10 mm nozzle onto a copper wheel rotating at 25 m/s. In order to obtain a homogeneous ribbon thickness below 50 µm, the argon ejection pressure was 200 mbar and nozzle-wheel gap distance was 0.5 mm [26, 27, 37, 38]. Within the scope of our study, 10 mm width and 30 µm thickness ribbons were produced.

Differential thermal analysis (DSC) analysis was performed with Mettler Toledo brand device to determine the crystallization temperature of rapid solidified NdFeB alloys. In order to ensure the crystallization of the amorphous structure in NdFeB-based ribbon alloys, the flash annealing was applied at temperatures of 680 °C and 710 °C, for 5 and 10 min and at a heating and cooling rate of 300 K/s. In addition, an external magnetic field of 5 Tesla was applied to some of the NdFeB alloys. The descriptions of the samples produced within the scope of the study are summarized in Table 2. X-ray diffraction (XRD) analysis performed from 20° to 80° of 2θ with a speed of 2°/min with Cu-Kα radiation to determine the crystal structure of the ribbons (PANalytical EMPYREAN). Scherer method was used to estimate the grain size [34, 39]. Vibrating sample magnetometer (VSM) analysis was performed on the Quantum Design PPMS DynaCool-9 to examine the magnetic properties of the NdFeB-based ribbons.

Table 1 The chemical composition of NdFeB magnet alloy

Elements	Nd	B	Si	Al	Fe
Content (wt%)	37.12	1.08	0.11	0.05	Balance

3 Results and discussion

Figure 1 shows the XRD patterns of NdFeB-based ribbon alloys produced by melt spinning method for the conditions melt-spun, flash annealed at 680 °C and 710 °C for 5 and 10 min and applied external magnetic field of 5 T. It is obvious that melt-spun ribbon alloys show a largely amorphous structure with trace amount crystalline phases. It is clearly seen that amorphous structures are obtained thanks to the rapid solidification by the melt spinning method. With the effect of rapid solidification, most of the structure became amorphous without forming a crystalline order [40]. In the melt spinning method, the rotation speed of the copper wheel, the ejection pressure and the distance the wheel-nozzle gap are important parameters that affect the cooling rate. Therefore, when the XRD results in Fig. 1 are evaluated; the parameters we have chosen for the production of amorphous ribbon show a successful result in line with the literature [26, 27]. It is clearly seen that the external magnetic field of 5 T has no effect on the crystal structure (AM sample). On the other hand, traces amount of $Nd_2Fe_{14}B$ hard magnetic phase at approximately 30° 2θ angle and α-Fe phase at 2θ = 44°angle are observed in melt spun samples. Intensities of sharp peaks of $Nd_2Fe_{14}B$ and α-Fe phases increase with applied flash annealing [31, 36]. It is clearly observed that the structure changes from amorphous characteristic to crystalline structure with the effect of temperature [12]. In addition, the intensity of the hard and soft magnetic crystal peaks increases with the increase of the duration [34, 41]. Temperature and a duration time are required for atoms to change from amorphous structure to a certain crystalline order [42, 43]. Due to the high atomic mobility at high temperatures and long duration times, atomic diffusion will become easier and the crystal sizes will increase. Therefore,

Table 2 Description of samples

A	AM	A680-5	A680M-5	A680-10	A710-5	A710-10
Melt spun	Melt spun + magnetized	Melt spun + flash annealed at 680 °C and 5 min	Melt spun + magnetized + flash annealed at 680 °C and 5 min	Melt spun + flash annealed at 680 °C and 5 min	Melt spun + flash annealed at 710 °C and 5 min	Melt spun + flash annealed at 710 °C and 10 min

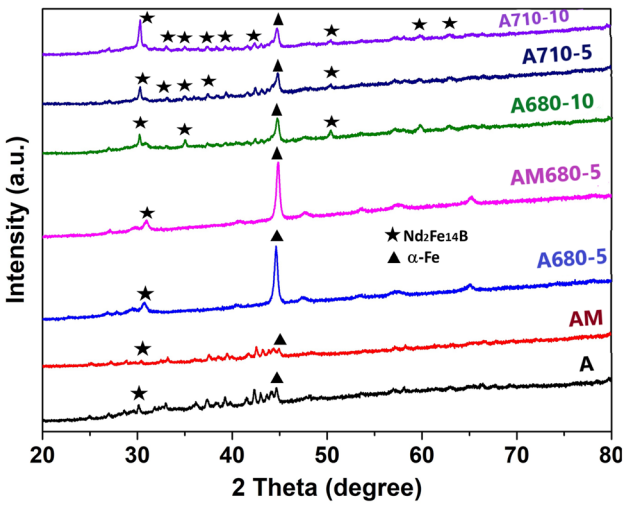

Fig. 1 XRD patterns of NdFeB alloy ribbons

flash annealing was applied to transformation from semi-amorphous structure to nanocrystallization. As a result, nanocrystalline grain structure was obtained thanks to flash annealing. It is known that nanocrystalline structures improve the magnetic properties of NdFeB magnets [34]. In addition, the Scherrer Equation was used to calculate the crystal sizes of the samples from the XRD patterns. The Scherrer Equation is expressed as [34, 44, 45]:

$$D = \frac{K\lambda}{\beta \cos\theta} \quad (1)$$

where K is the Scherrer constant (about 0.94 for cubic crystal systems); β is the with of the X-ray peak, measured as full width at half maximum (FWHM) of respective peaks; λ is the X-ray wavelength (1.5406 Å for Cu-K α) and is the Bragg angle of the X-rays. According to the calculation, the crystalline size distribution (D) in the melt-spun alloys obtained between 20 and 50 nm. For the A710-10 sample, estimated average crystal size of the $Nd_2Fe_{14}B$ phase at $2\theta = 30°$ was 30 nm, while the α-Fe phase at $2\theta = 44°$ was 50 nm.

Figure 2 shows the transformation during heating from 200 to 400 °C at a constant heating rate of 5 °C/min. More crystallization events are exhibited in A and AM samples, seen from the exothermic reaction peaks. The crystallization temperature increased by about 15 °C with the external magnetic field. However, the external magnetic field did not have any effect on the flash annealed samples. Small exothermic peaks are observed in the flash annealed samples at 680 °C and 710 °C. Due to the short-term annealing process, the amorphous structure did not crystallize completely. It is clearly seen from the DSC results that the residual amorphous phase is still present in the structure. XRD results also support DSC results as the phase peaks are not sharp and intense. These results agree with many researches in the literature [34, 46]. Hamano et al. observed residual amorphous structures in the sample annealed at 700 °C for 3 min [46]. It is clearly seen that the amorphous structure present in the material is not fully crystallized by the flash annealing process. These residual amorphous structures are known to inhibit crystal growth [46, 47]. Accordingly, it can be said that the crystal

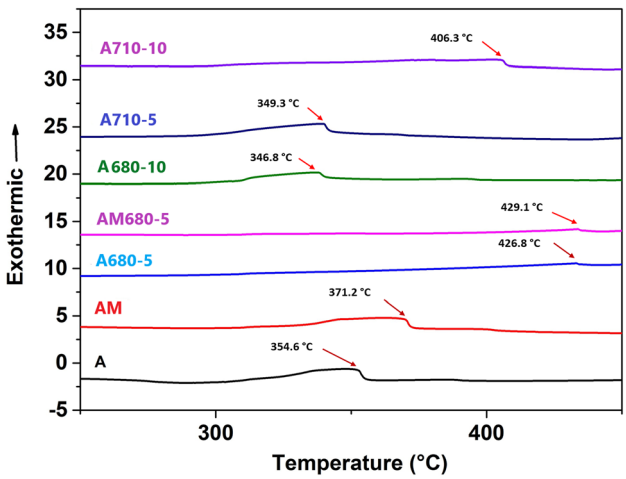

Fig. 2 DSC curves of melt-spun NdFeB alloys

size remains at nanoscale. When DSC results are interpreted together with XRD results; while α-Fe phase formation was more with flash annealing at 680 °C, $Nd_2Fe_{14}B$ phase formation was more with flash annealing at 710 °C. It is clearly seen that the XRD results support the DSC results.

In Fig. 3, the magnetic hysteresis loops of the melt-spun NdFeB-based alloys. According to magnetic hysteresis loops, magnetic saturation of sample A was lowest without flash annealing. As can be seen from the XRD results, the α-Fe soft magnetic phase, which increases the magnetic saturation in hard magnetic materials, is quite low in the semi-amorphous sample A. The magnetic saturation of sample A was found to be low due to the effect of rapid solidification, since there was not enough crystallization and the α-Fe soft magnetic phase was insufficient. In hard magnetic magnets, magnetic saturation is related to the amount of soft magnetic phase and the crystal size. With flash annealing applied to semi-amorphous ribbons, atomic mobility was increased and thus crystallization was achieved. Therefore, magnetic saturation increases with flash annealing process. The maximum magnetic saturation was observed as 117.58 emu/g in the flash annealed sample at 680 °C for 5 min (A680-5). As can be seen from the XRD results, the amount of α-Fe soft magnetic phase increased significantly in the A680-5 sample. The α-Fe soft magnetic phase is known to increase magnetic saturation in NdFeB-based hard magnetic magnets [48]. On the other hand, with the extension of the time to 10 min, the amount of hard magnetic phase increased and thus the magnetic saturation slightly decreased. In addition, it is clearly seen in the XRD results that the $Nd_2Fe_{14}B$ hard magnetic phases more formed with flash annealing at 710 °C. Depending on this, the magnetic saturation of the samples flash annealed at 710 °C is lower than flash annealed at 680 °C.

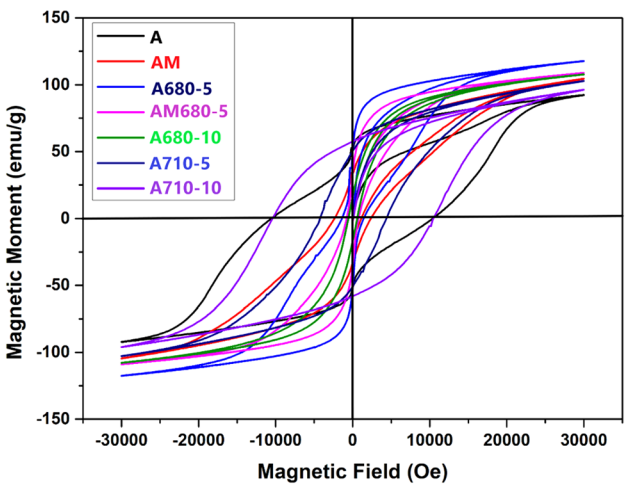

Fig. 3 Magnetic hysteresis loops of the NdFeB samples

The high coercivity of hard magnetic materials directly affects the magnet properties [34]. In addition, the coercivity of permanent magnets is related to the size and amount of the soft and hard magnetic phases and the strength of the exchange coupling between them [49]. Within the scope of our study, the maximum coercivity was obtained in the A sample. The closest result was obtained by flash annealing for 10 min at 710 °C. Because the hard magnetic phase, which was more in the A and A710-10 samples compared to the other samples, increased the coercivity significantly. It can be understood from the XRD results, the soft magnetic phases could not crystallize sufficiently due to the rapid solidification in sample A. Therefore, the intensity of the hard magnetic phases is higher than the soft magnetic phase. In addition, XRD results show that both soft and hard magnetic phases are formed in the A710-10 sample with the effect of temperature. In fact, in flash annealing at 710 °C, it is expected that the coercivity will decrease with the formation of the soft magnetic phase. However, here, it is seen that the exchange coupling mechanism between the hard magnetic phases and the soft magnetic phases is dominant [50]. On the other hand, a significant reduction in coercivity was observed in flash annealed samples at 680 °C. Because the α-Fe phase intensity, which is the soft magnetic phase, increased in A680-5 and A680-10 samples. It is known from previous researches that soft magnetic phases reduce coercivity [49, 51]. Schrefl et al. stated that the coercivity of permanent magnets improves as the amount and size of the soft magnetic phase increases [49]. It was also observed that the relatively high Nd content did not significantly affect the coercivity [29, 35]. In this context, the coercivity results compatible with the literature.

The exchange coupling between the hard and soft magnetic phases causes the magnetic moment of the soft magnetic grains to rotate throughout the hard magnetic grain boundaries. This improves the magnetic permanence properties of permanent magnets and accordingly offers better hard magnetic properties [H_c and $(BH)_{max}$ etc.] [51]. In addition, HREEs such as Dy and Tb used in NdFeB magnets are

known to decrease magnetic remanence while improving coercivity [52]. As a result, the maximum energy product important for permanent magnet property is reduced [52]. A relatively high magnetic remanence was obtained within the scope of our study. The highest magnetic remanence value in the sample flash annealed at 710 °C for 10 min was 57.64 emu/g. Sample A is closest to this value. It can be said that the exchange coupling mechanism between the soft and hard magnetic phases works effectively in the sample applied flash annealing at 710 °C for 10 min. According to the XRD results in Fig. 1, the remanence values were lower in the A sample due to the more hard magnetic phases and to be predominance of the amorphous structure. On the other hand, magnetic remanence was found to be low in all of the samples flash annealed at 680 °C due to the dominant soft magnetic phase. Chen et al., in their study in 2019, noticed that the magnetic remanence decreased with the increase of the soft magnetic phase, and a similar result was seen in our study [53] (Fig. 4).

It can be listed in Table 3 with the magnetic saturation (B_s), coercivity (H_c), magnetic remanance (B_r), and maximum energy product [$(BH)_{max}$] for each melt-spun alloy. According to Table 2, A710-10 alloy presents relatively high hard magnetic properties [H_c, B_r and $(BH)_{max}$] depending on the flash annealing at 710 °C and 10 min. Because, it can be abovementioned, optimum soft and hard magnetic phase grain size is achieved by the flash annealing, hence the exchange coupling mechanism between $Nd_2Fe_{14}B$ and α-Fe is improved [5, 54]. Although HREEs such as Dy, Tb and Pr are not used in NdFeB magnet alloy, magnetic remanence is improved because the Nd ratio is high. According to Zhang, HREEs reduce the maximum energy product as they reduce magnetic saturation [52]. In addition, with the applied flash annealing process, the interaction of soft and hard magnetic phases has been improved and its coercivity increased. Thus, the maximum energy product of the flash annealed sample at 710 °C for 10 min was 87.79 kJ/m^3. This value is much better than the $(BH)_{max}$ obtained in many studies in the literature [55, 56]. On the other hand, due to the semi-amorphous structure formed by the rapid solidification in sample A, the exchange coupling mechanism could not work. A similar situation is observed in A680-5 and A680-10 samples, which were flash annealed at 680 °C and dominated by the soft magnetic phase.

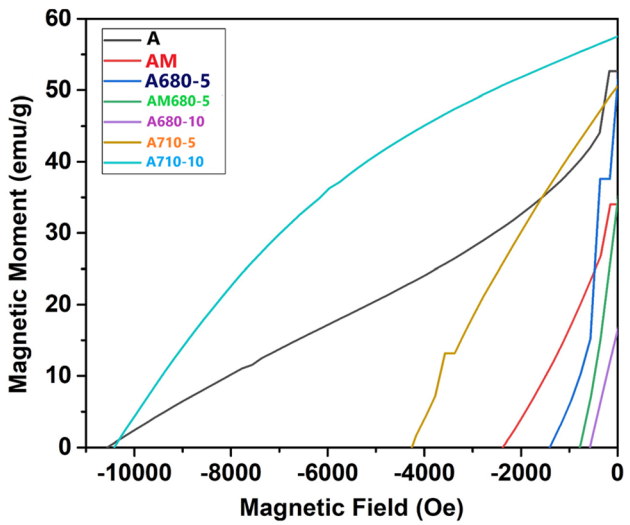

Fig. 4 Second-quadrant demagnetization curve of samples

4 Conclusion

In this study, relatively high Nd ratio NdFeB magnet alloys were produced with melt spinning, which is a rapid solidification method. In addition, the effect of flash annealing and magnetization processes applied to various samples were investigated. Semi-amorphous structures were obtained by melt spinning method. It has been observed that most amorphous structures crystallize at nanoscale with flash annealing at 680 °C and 710 °C for different durations of 5 and 10 min.

According to the XRD results, melt-spun plain samples are in semi-amorphous structure. In addition, the average crystal size distribution in melt-spun samples is between 20 and 50 nm. With the flash annealing process at 680 °C, the soft magnetic α-Fe phase became more dominant. $Nd_2Fe_{14}B$ hard magnetic phase was formed mostly with the flash annealing process at 710 °C.

According to the DSC results, various exothermic crystallization reaction peaks were observed between the temperatures of 350 °C and 430 °C.

The highest magnetic saturation was obtained as 117.58 emu/g in the sample flash annealed at 680 °C for 5 min. The best magnetic remanence value was 57.64 emu/g in the sample flash annealed at 710 °C for 10 min. The coercivity value of the same sample was also quite high as 10,419.07 Oe. The maximum energy product improved thanks to the high

Table 3 Magnetic properties of samples

Melt-spun alloy	Saturation magnetization (B_s), emu/g	Magnetic remanence (B_r), emu/g	Coercivity (H_c), Oe	Maximum energy product $(BH)_{max}$, kJ/m^3
A	92.41	52.86	10,667.98	43.16
AM	104.59	34.019	2306.2	12.62
A680-5	117.58	54.308	1453.13	9.36
A680M-5	108.990	36.53	805.21	4.08
A680-10	107.83	15.22	591.334	28.29
A710-5	102.74	52.65	4514.75	34.11
A710-10	96.34	57.64	10,419.07	87.79

remanence and coercivity, important for NdFeB magnets resulted in a considerably high value of 87.79 kJ/m3 in the sample flash annealed at 710 °C for 10 min. As a result, NdFeB melt-spun alloys produced without using HREEs and flash annealed at 710 °C for 10 min are candidates for many magnet applications.

Acknowledgements

This study was funded by the Scientific and Technological Research Council of Turkey (TUBITAK) with Project Number of 216M252 and Scientific Research Projects Coordinator of Sivas University of Science and Technology with Project Number of 2020-TDP-Mühe-0001.

Authors contributions

All authors contributed to the study conception and design. Material preparation, data collection and analysis were performed by MFK, YY, HT and BA. The first draft of the manuscript was written by YY and BA. All authors commented on previous versions of the manuscript. All authors read and approved the final manuscript.

Data availability

All data generated or analysed during this study are included in this published article (and its supplementary information files).

Declarations

Conflict of interest The authors declare that they have no competing financial interests or personal relationships that could have seem to influence the study reported in this paper.

References

1. D.F. Cygan, M.J. McNallan, J. Magn. Magn. Mater. **139**, 131 (1995)
2. R.W. McCallum, L. Lewis, R. Skomski, M.J. Kramer, I.E. Anderson, Annu. Rev. Mater. Res. **44**, 451 (2014)
3. H. Nakamura, Scr. Mater. **154**, 273 (2018)
4. S.U. Rehman, Q. Jiang, L. He, M. Ghazanfar, W. Lei, X. Hu, S.U. Awan, S. Ma, Z. Zhong, J. Magn. Magn. Mater. **466**, 277 (2018)
5. H. Zhao, H. Liu, J. Su, J. Rare Earths **24**, 379 (2006)
6. M. Lv, T. Kong, W. Zhang, M. Zhu, H. Jin, W. Li, Y. Li, J. Magn. Magn. Mater. **517**, 167278 (2021)
7. B.B. Straumal, A.R. Kilmametov, A.A. Mazilkin, S.G. Protasova, K.I. Kolesnikova, P.B. Straumal, B. Baretzky, Mater. Lett. **145**, 63 (2015)
8. W.G. Sawyer, N. Argibay, D.L. Burris, B.A. Krick, Annu. Rev. Mater. Res. **44**, 395 (2014)
9. X. Lin, Y. Luo, H.J. Peng, Y.F. Yang, Y.K. Dou, Z.L. Wang, K.S. Xu, S.L. Diao, D.B. Yu, J. Magn. Magn. Mater. **490**, 165–454 (2019)
10. B.B. Straumal, A.A. Mazilkin, S.G. Protasova, D.V. Gunderov, G.A. López, B. Baretzky, Mater. Lett. **161**, 735 (2015)
11. K.H. Müller, W. Grünberger, D. Hinz, B. Gebel, D. Eckert, A. Handstein, Mater. Lett. **34**, 50 (1998)
12. M. Zhang, W. Zhang, F. Chen, Y. Guo, F. Li, W. Liu, J. Supercond. Nov. Magn. **31**, 2811 (2018)

13. J. Pyrhönen, S. Ruoho, J. Nerg, M. Paju, S. Tuominen, H. Kankaanpää, R. Stern, A. Boglietti, N. Uzhegov, IEEE Trans. Ind. Electron. **62**, 857 (2015)
14. J.M.D. Coey, Scr. Mater. **67**, 524 (2012)
15. C. Chen, Y.L. Huang, Y.F. Yao, X.K. Fu, W. Li, Y.H. Hou, J. Magn. Magn. Mater. **530**, 9 (2021)
16. Y.L. Li, Z.X. Dou, X.M. Chen, K. Lv, F.S. Li, X.D. Hui, J. Alloys Compd. **844**, 155767 (2020)
17. J. Zheng, M. Jiang, L. Qiao, J. Sheng, J. Li, L. Jiang, Mater. Lett. **62**, 4407 (2008)
18. D. Brown, B.M. Ma, Z. Chen, J. Magn. Magn. Mater. **248**, 432 (2002)
19. Y. Yang, A. Walton, R. Sheridan, K. Güth, R. Gauß, O. Gutfleisch, M. Buchert, B.M. Steenari, T. Van Gerven, P.T. Jones, K. Binnemans, J. Sustain. Metall. **3**, 122 (2017)
20. M.R. Zion (2019).
21. J. Li, Y. Bian, K. Xu, X. Xie, J. Ni, C. Hu, S. Zhou, Mater. Lett. **267**, 127537 (2020)
22. H.C. Hua, G.Y. Wang, C.H. Zheng, G.X. Huang, Q.Z. Xu, L.H. Wu, S.Y. Shi, Mater. Lett. **7**, 65 (1988)
23. I.S. Tereshina, I.A. Pelevin, E.A. Tereshina, G.S. Burkhanov, K. Rogacki, M. Miller, N.V. Kudrevatykh, P.E. Markin, A.S. Volegov, R.M. Grechishkin, S.V. Dobatkin, L. Schultz, J. Alloys Compd. **681**, 555 (2016)
24. X.H. Li, Y. Guan, W. Li, J.W. Zhang, X.Y. Zhang, Mater. Lett. **61**, 2728 (2007)
25. M. F. Kılıçaslan, Y. Yılmaz, and B. Akgül, Eur. J. Sci. Technol. **39**, 9–12 (2022).
26. V.I. Tkatch, A.I. Limanovskii, S.N. Denisenko, S.G. Rassolov, Mater. Sci. Eng. A **323**, 91 (2002)
27. A.A. Shirzadi, T. Kozieł, G. Cios, P. Bała, J. Mater. Process. Technol. **264**, 377 (2019)
28. W.F. Li, T. Ohkubo, K. Hono, M. Sagawa, J. Magn. Magn. Mater. **321**, 1100 (2009)
29. J. Liu, H. Sepehri-Amin, T. Ohkubo, K. Hioki, A. Hattori, T. Schrefl, K. Hono, Acta Mater. **61**, 5387 (2013)
30. C. Ma, J. Xia, X. Zhang, Y. Zhou, A. Morisako, S.N. Piramanayagam, X. Liu, J. Magn. Magn. Mater. **474**, 406 (2019)
31. R.K. Murakami, V. Villas-Boas, Mater. Res. **2**, 67 (1999)
32. Z.H. Hu, F.Z. Lian, M.G. Zhu, W. Li, J. Magn. Magn. Mater. **320**, 1735 (2008)
33. R.S. Keri, V. Adimule, P. Kendrekar, B.S. Sasidhar, Top. Catal. (2022). https://doi.org/10.1007/s11244-022-01562-0
34. S. Caglar, M.F. Kilicaslan, A. Atasoy, H. Tiryaki, M. Erkovan, S. JikHong, J. Mater. Sci. Mater. Electron. **32**, 2338 (2021)
35. M. Leonowicz, H.A. Davies, Mater. Lett. **19**, 275 (1994)
36. M.V.P. Altoé, M. Chandramouli, G. Thomas, J. Appl. Phys. **79**, 4846 (1996)
37. M.F. Kılıçaslan, Y. Yılmaz, B. Akgül, H. Karataş, C.D. Vurdu, Adv. Mater. Sci. **21**, 79 (2021)
38. B. Majumdar, D. Akhtar, V. Chandrasekaran, in *Trans. Indian Inst. Met.* (2007), pp. 343–347.
39. H. Köçkar, Ö. Şenturk, A. Karpuz, O. Karaagac, N. Kaplan, H. Kuru, J. Supercond. Nov. Magn. **32**, 3535 (2019)
40. Z.Y. Zhang, L.Z. Zhao, X.C. Zhong, D.L. Jiao, Z.W. Liu, J. Magn. Magn. Mater. **441**, 429 (2017)
41. X.Y. Zhang, Y. Guan, J.W. Zhang, Appl. Phys. Lett. **80**, 1966 (2002)
42. W.D. Callister, D.G. Rethwisch, *Materials Science and Engineering: An Introduction*, 10th edn. (Wiley, New York, 2018)
43. R.E. Simpson, P. Fons, A.V. Kolobov, T. Fukaya, M. Krbal, T. Yagi, J. Tominaga, Nat. Nanotechnol. **6**, 501 (2011)
44. M. Kamal, E.S. Gouda, Mater. Manuf. Process. **21**, 736 (2006)
45. F.T.L. Muniz, M.A.R. Miranda, C. Morilla Dos Santos, J.M. Sasaki, Acta Crystallogr. Sect. A **72**, 385 (2016)
46. M. Hamano, M. Yamasaki, H. Mizuguchi, T. Kobayashi, H. Yamamoto, and A. Inoue, MRS Proc. **577** (1999)
47. M. Yamasaki, M. Hamano, H. Mizuguchi, T. Kobayashi, K. Hono, H. Yamamoto, A. Inoue, Scr. Mater. **44**, 1375 (2001)
48. V. Swaminathan, P.K. Deheri, S.D. Bhame, R.V. Ramanujan, Nanoscale **5**, 2718 (2013)
49. T. Schrefl, J. Fidler, H. Kronmüller, Phys. Rev. B **49**, 6100 (1994)
50. W.C. Chang, S.H. Wu, B.M. Ma, C.O. Bounds, J. Magn. Magn. Mater. **167**, 65 (1997)
51. Y. Wang, C. You, J. Wang, N. Tian, Z. Lu, L. Ge, J. Rare Earths **30**, 757 (2012)
52. Y. Zhang, X. Xu, J. Supercond. Nov. Magn. **34**, 2711 (2021)
53. X. Chen, C. Cen, L. Zhou, R. Cao, Z. Yi, Y. Tang, J. Magn. Magn. Mater. **483**, 152 (2019)
54. Z. Wang, H. Xu, J. Ni, Q. Li, B. Zhou, Rare Met. **25**, 337 (2006)
55. C. Kurniawan, A. S. Purba, E. A. Setiadi, S. Simbolon, A. Warman, and P. Sebayang, in *J. Phys. Conf. Ser.* (2018).
56. M. Hussain, J. Liu, L.Z. Zhao, X.C. Zhong, G.Q. Zhang, Z.W. Liu, J. Magn. Magn. Mater. **399**, 26 (2016)